Earth and Planetary Science Letters 548 (2020) 116501

Contents lists available at ScienceDirect

Earth and Planetary Science Letters

www.elsevier.com/locate/epsl

Deglaciation of Pope Glacier implies widespread early Holocene ice sheet thinning in the Amundsen Sea sector of Antarctica

Joanne S. Johnson [a,*], Stephen J. Roberts [a], Dylan H. Rood [b], David Pollard [c], Joerg M. Schaefer [d], Pippa L. Whitehouse [e], Louise C. Ireland [a], Jennifer L. Lamp [d], Brent M. Goehring [f], Cari Rand [f], James A. Smith [a]

[a] British Antarctic Survey, High Cross, Madingley Road, Cambridge CB3 0ET, UK
[b] Department of Earth Science & Engineering, Imperial College London, London SW7 2AZ, UK
[c] Earth and Environmental Systems Institute, Pennsylvania State University, University Park, PA 16802, USA
[d] Lamont-Doherty Earth Observatory, Columbia University, Route 9W, Palisades, New York NY10964, USA
[e] Department of Geography, Durham University, Durham, UK
[f] Department of Earth & Environmental Sciences, Tulane University, New Orleans, LA 70118, USA

ARTICLE INFO

Article history:
Received 16 August 2019
Received in revised form 8 June 2020
Accepted 24 July 2020
Available online xxxx
Editor: J.-P. Avouac

Keywords:
Holocene
glaciation
Antarctica
Amundsen Sea Embayment
cosmogenic isotopes
geomorphology

ABSTRACT

The Amundsen Sea sector of the Antarctic ice sheet presently dominates the contribution from Antarctica to sea level rise. Several large ice streams that currently drain the sector have experienced rapid flow acceleration, grounding line retreat and thinning during the past few decades. However, little is known of their longer-term – millennial-scale – retreat history, despite the reliance of several ice sheet and glacial-isostatic adjustment models on such data for improving sea level prediction from this critical region. This study investigates the timing and extent of surface lowering of one of those ice streams, Pope Glacier, since the Last Glacial Maximum (LGM), using glacial-geological evidence for former ice cover. We present a new deglacial chronology for the glacier, derived from surface exposure dating of glacially-deposited cobbles and ice-scoured bedrock from Mount Murphy and its surrounding peaks. Cosmogenic ^{10}Be exposure ages from 44 erratic cobbles and 5 bedrock samples, and in situ ^{14}C exposure ages from one erratic and 8 bedrock samples are predominantly in the range 5.5-16 ka. Although ^{10}Be inheritance from prior exposure is prevalent in some erratics and probably all bedrock samples, none of the ages predate the LGM. From these results we infer that the surface of Pope Glacier lowered by 560 m during the early- to mid-Holocene (9-6 ka), at an average rate of 0.13 ± 0.09/0.04 m yr^{-1}. The lowering coincided with a period of enhanced upwelling of warm Circumpolar Deep Water onto the continental shelf in the region. A reduction in buttressing — facilitated by such upwelling — by an ice shelf that is thought to have spanned the embayment until 10.6 cal kyr BP could have triggered simultaneous early Holocene thinning of Pope Glacier and glaciers elsewhere in the Amundsen Sea Embayment.

1. Introduction

The West Antarctic Ice Sheet (WAIS), and particularly its Amundsen Sea sector, is key to sea level prediction because it rests on bedrock that is, in places, more than 1000 m below sea level and deepens towards the centre of the ice sheet. This makes the WAIS potentially vulnerable to runaway retreat (Schoof, 2007). Moreover, the Amundsen Sea sector of WAIS contains enough water to make a future contribution to sea level rise of up to 1.5 m (Rignot et al., 2019), a magnitude that would have major economic and societal consequences, particularly if it occurred over the next few centuries (Favier et al., 2014; Yu et al., 2018).

In the past few decades satellite observations have revealed that the WAIS in the Amundsen Sea Embayment (ASE) is experiencing significant thinning (Pritchard et al., 2009; Shepherd et al., 2019), flow acceleration (Rignot et al., 2011a, 2011b; Mouginot et al., 2014) and rapid grounding line retreat (Rignot et al., 2014). Since then, much research has focused on understanding the factors driving those changes, particularly for Pine Island Glacier in the eastern ASE (e.g. Jenkins et al., 2016; Hillenbrand et al., 2017; Smith et al., 2017). However, simultaneously, changes in WAIS at rates comparable to or in excess of those for Pine Island Glacier have been occurring in the central ASE, on the Thwaites, Smith, Kohler and Pope Glaciers (e.g. Pritchard et al., 2009; Mouginot et

* Corresponding author.
E-mail address: jsj@bas.ac.uk (J.S. Johnson).

https://doi.org/10.1016/j.epsl.2020.116501

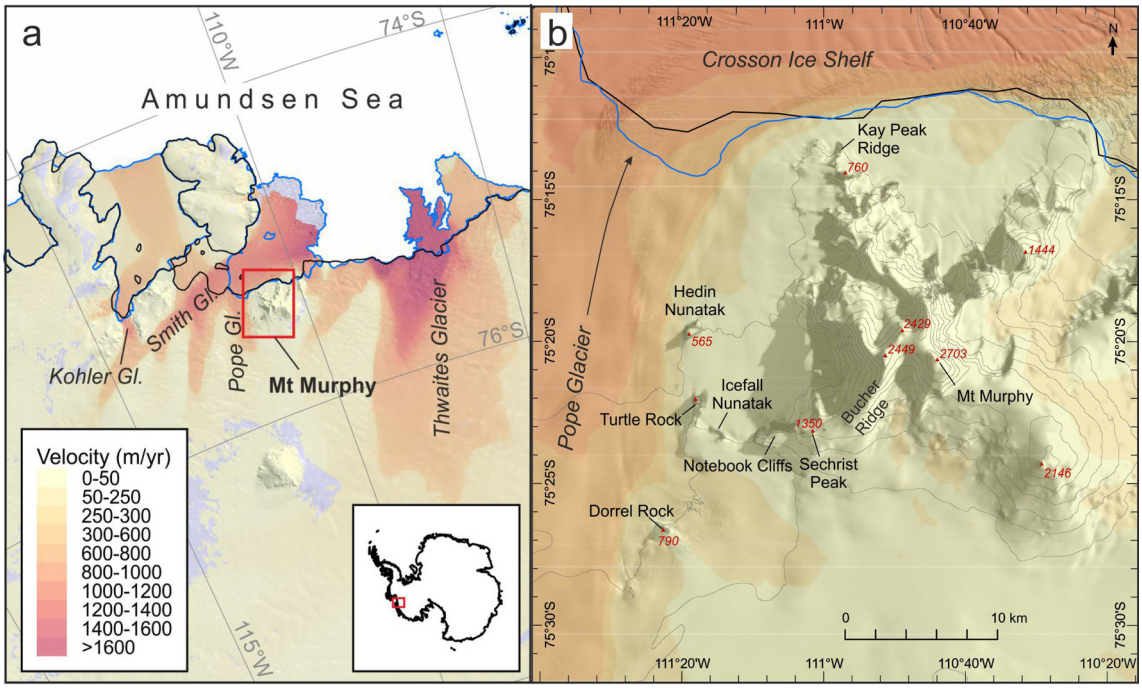

Fig. 1. Location of study area. a. Location of Mt Murphy and Pope Glacier in relation to ice streams of the central ASE. The red box in the inset shows location in Antarctica, and the red box labelled Mt Murphy in the main panel shows the location of panel b. b. Location of study sites around Mt Murphy. Contours are in 200 m intervals. Scale is 1:50,000. In both panels, ice velocities (Rignot et al., 2011a, 2011b) are overlain on the Landsat Image of Antarctica (LIMA). The grounding line (black) is from Rignot et al. (2011c), and the coastline (blue) from the Antarctic Digital Database version 6. (For interpretation of the colours in the figure(s), the reader is referred to the web version of this article.)

al., 2014; Rignot et al., 2019). This gives rise to concern that the thinning, flow and retreat of those glaciers will likewise continue to accelerate over coming decades.

Several modelling approaches for predicting the rate and timing of future ice loss from Antarctica rely heavily on well-constrained records of past ice sheet change for validation (e.g. Briggs and Tarasov, 2013; Pollard et al., 2016). Long-term (centennial- to millennial-scale) records for validating such models must be obtained through acquisition of field data because satellite observations of ice surface elevation from before the early 1960s do not exist. The primary aim of this study is therefore to provide a chronological record of changes in ice sheet thickness since the Last Glacial Maximum (LGM) in the central ASE, derived from surface exposure dating of glacial deposits. We focus on a series of nunataks situated adjacent to Pope Glacier (Fig. 1a) which, together with the Smith and Kohler Glaciers, contributes 23 % of the current ice mass loss from the ASE (Mouginot et al., 2014). Substantial retreat of its grounding line in recent years suggests Pope Glacier is experiencing the same instability as Thwaites Glacier (Rignot et al., 2014). As yet, only a handful of terrestrial constraints on former ice sheet thickness exist from this important region (Johnson et al., 2008, 2017; Lindow et al., 2014); consequently, uncertainties on model predictions of future sea level rise resulting from this part of the ASE are still large (Yu et al., 2018).

2. Background and regional setting

A review of Quaternary ice sheet history of the whole ASE encompassing both the marine and terrestrial realm is given in Larter et al. (2014). Subsequent glacial-geological studies have provided evidence that: i) grounding line retreat in the eastern ASE occurred with similar style and timing as in the central ASE, with retreat onto the inner continental shelf by the early Holocene (10.6 cal kyr BP; Smith et al., 2014); ii) extremely rapid thinning of Pine Island Glacier occurred a few thousand years later, in the early Holocene (~8 ka; Johnson et al., 2014); and iii) complete deglaciation of Bear Peninsula – situated adjacent to the Dotson Ice Shelf – had also occurred in the early Holocene, by 9.6 ka (Johnson et al., 2017).

However, there is still a notable lack of terrestrial glacial-chronological data from the Thwaites Glacier catchment in the central ASE. One of the reasons for this is the corresponding lack of ice-free nunataks in the region, especially at the margins of Thwaites Glacier itself. The largest peak in the ASE that is not entirely ice-covered at present is Mt Murphy, a large volcanic edifice. This is bounded by Crosson Ice Shelf to the north and Pope Glacier – a tributary of Smith Glacier – to the west (Fig. 1a). At times in the past when the WAIS was more extensive than at present (such as at the LGM; Larter et al., 2014), Pope Glacier would have been a tributary of the neighbouring Thwaites Glacier, and thus changes in its thickness would likely reflect changes in the grounding line position of Thwaites Glacier. The lower flanks of Mt Murphy and several peaks that surround it are presently ice-free, and support glacial deposits that provide information on past ice sheet configuration. The present study uses surface exposure dating of glacial deposits to determine the timing of deglaciation following retreat of ice since the last glacial period. The exposure dating method makes use of the fact that cosmogenic isotopes, such as ^{10}Be, accumulate within rock surfaces only during ice-free periods or periods of very thin ice cover. Therefore, the timing and pace of ice thinning at a site can be derived from the concentrations of these isotopes in the surfaces of bedrock and glacially-transported cobbles collected from a range of altitudes. A similar "dipstick" approach has been used in several other studies of the WAIS (e.g. Stone et al., 2003; Ackert et al., 2011; Johnson et al., 2014).

3. Study area

Mount Murphy is a stratovolcano constructed on a north-sloping fault-block massif of pre-Cenozoic volcanic basement (Smellie, 2001). All but one of the nunataks surrounding it – Icefall

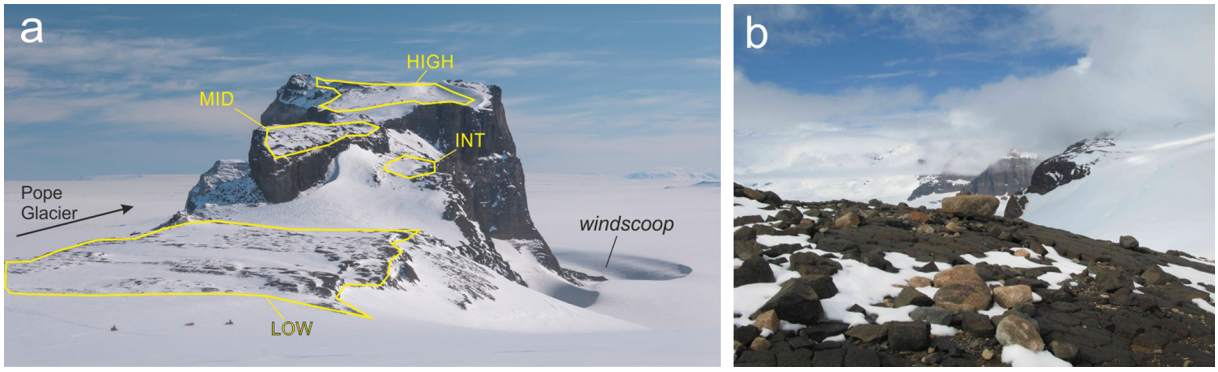

Fig. 2. Study sites on Turtle Rock. a. Turtle Rock from the south. Two snowmobiles and a sledge in left foreground for scale. Samples were collected from the four areas shown in yellow. b. Numerous quartz-bearing erratic cobbles and boulders perched on basaltic bedrock of the "LOW" terrace.

Nunatak, Notebook Cliffs, Turtle Rock, and Hedin Nunatak (Fig. 1b) – are composed of basalt lava flows which were formed during volcanic eruptions 9.2-0.6 Ma ago (LeMasurier et al., 1994). In addition, an older intrusive igneous body (34 Ma; Wilch, 1997) outcrops on its south-western side (Dorrel Rock; Fig. 1b). The nunataks from which samples were collected for this study have been described in detail by others (LeMasurier et al., 1994; Smellie, 2001; Wilch and McIntosh, 2002) and are therefore summarised only briefly here.

3.1. Turtle Rock

Turtle Rock consists of at least two superimposed hyaloclastite lava sequences, with overlying vesicular capping lavas, rising to a summit at 712 m above sea level (asl). The capping lavas have an $^{40}Ar/^{39}Ar$ eruption age of 4.70 $\pm$ 0.15 Ma (Wilch and McIntosh, 2002); the lowermost sequence presently forms a relatively flat terrace at 440-450 m asl and was erupted at 5.95 $\pm$ 0.6 Ma (Wilch, 1997). The nunatak is largely ice-free, except for a broad area above the lowermost terrace. A concave area near the summit has persistent snow-cover, but elsewhere surfaces are heavily windswept by the prevailing winds. A prominent windscoop is present around the base of the peak on its north-eastern side (Fig. 2a). The only pre-existing surface exposure ages from the whole Mt Murphy area were measured in 3 granite cobbles situated on the uppermost slopes of Turtle Rock (Johnson et al., 2008; the area labelled as "HIGH" in Fig. 2a).

3.2. Icefall Nunatak-Notebook Cliffs-Bucher Ridge

Between Mt Murphy and Turtle Rock, a series of volcanic terraces rises to a large flat-topped volcanic mesa at ~900 m asl and higher to a tuff cone at Sechrist Peak (Fig. 1b). These form an approximately east-west-trending series of outcrops bounded on the western side by a steep icefall. On the eastern side, a gently-sloping ridge comprising basalt and trachyte lavas rises from approximately 1300 m asl to Bucher Peak and steepens beyond that to the summit of Mt Murphy at 2703 m asl. Together, these landforms comprise a sequence which is referred to here as the Icefall Nunatak-Notebook Cliffs-Bucher Ridge sequence; it is oriented perpendicular to the flow direction of Pope Glacier (Fig. 1b). Icefall Nunatak consists of basaltic lavas and breccias (Smellie, 2001) erupted between 6.80-6.52 Ma (Wilch and McIntosh, 2002). Sechrist Peak was emplaced at 590 ka (LeMasurier et al., 1994). A few degraded basaltic scoria cones outcrop along Bucher ridge.

3.3. Dorrel Rock

Dorrel Rock is a 34 Ma-old coarse-grained gabbroic outcrop measuring 750 by 350 m, and is cross-cut by E-W-trending dykes of trachyte and benmoreite (Rocchi et al., 2006). It is situated at the confluence of Pope Glacier and one of its tributaries, 25 km upstream of the modern grounding line (Fig. 1b).

3.4. Kay Peak ridge

An exposed rocky ridge extends 2.3 km northward of Kay Peak towards the Crosson Ice Shelf (Fig. 1b), terminating 1.5 km from the modern grounding line. It consists of gneiss bedrock exposed from the modern ice sheet surface at 70 m asl up to 332 m asl, above which the gneiss is interbedded with a diamict and basalt. The diamict is extensively eroded, resulting in a scattering of rounded cobbles derived from it over the gneiss bedrock surface below.

4. Methods

4.1. Sampling strategy

Satellite imagery was used prior to the field campaign (December 2015-January 2016) to identify sites likely to support erratic cobbles and boulders based on slope angle and presence of visible drift. Some sites were already known to be strewn with glacial erratics (e.g. Turtle Rock; Johnson et al., 2008). Due to its relatively high elevation above the present ice sheet surface (rising to 2450 m asl) and large altitudinal range, Bucher Ridge (Fig. 1b) was identified as the only site which might record the maximum thickness of the LGM ice sheet.

A total of 148 rock samples were collected (122 erratics and 26 bedrock) from several nunataks and ridges surrounding Mt Murphy (Fig. 1b). Of these, a suite of 44 erratic cobbles and boulders and 10 bedrock samples (Table 1) were selected for surface exposure dating based on their geomorphic setting, altitude and location. These cover a sufficiently large elevation range above the modern ice sheet surface to permit determination of a detailed thinning trajectory for Pope Glacier. Wherever possible, boulders and cobbles were prioritised over bedrock for dating, to minimize the chance of incurring problems with inherited ^{10}Be from prior exposure (see Stone et al., 2003 and Balco, 2011). Where no quartz-bearing erratics were present, striated bedrock was collected. Although in some areas, such as Kay Peak ridge (Fig. 1b), bedrock is quartz-bearing and therefore suitable for both cosmogenic ^{10}Be and ^{14}C dating, the majority of sites with striated bedrock are basaltic. Developments in extraction of cosmogenic ^{14}C from non-quartz-bearing lithologies may permit exposure dating of the basaltic samples in future (Pigati et al., 2010).

Position and elevation measurements for each sample were made using a Trimble GPS 5700 receiver. The GNSS observationswere post-processed using Precise Point Positioning in Bernese

Table 1
Sample details and location information.

Sample ID	BAS#	Date collected	Location	Type	Latitude	Longitude	Altitude (m a.s.l.)	Shielding factor	Reference
TR1	R5.403.1	2006	Turtle Rock high	erratic	−75.3690	−111.2991	700	0.991	Johnson et al. (2008)
TR2	R5.404.1	2006	Turtle Rock high	erratic	−75.3707	−111.2912	635	0.985	Johnson et al. (2008)
TR3	R5.404.2	2006	Turtle Rock high	erratic	−75.3711	−111.2897	633	0.994	Johnson et al. (2008)
TUR-120	R15.5.3	this study	Turtle Rock middle	erratic	−75.3753	−111.3005	567	0.999	–
TUR-121	R15.6.1	this study	Turtle Rock high	erratic	−75.3704	−111.2906	643	0.996	–
TUR-123	R15.6.3	this study	Turtle Rock high	erratic	−75.3706	−111.2923	639	0.993	–
TUR-124	R15.6.4	this study	Turtle Rock high	erratic	−75.3705	−111.2908	641	0.989	–
TUR-125	R15.6.5	this study	Turtle Rock high	erratic	−75.3699	−111.2908	661	0.982	–
TUR-127	R15.6.7	this study	Turtle Rock high	erratic	−75.3694	−111.2984	679	0.986	–
TUR-129	R15.6.9	this study	Turtle Rock high	erratic	−75.3691	−111.2975	683	0.997	–
TUR-130	R15.6.10	this study	Turtle Rock high	erratic	−75.3697	−111.2965	681	1.000	–
TUR-118	R15.5.1	this study	Turtle Rock middle	erratic	−75.3757	−111.3018	568	0.993	–
TUR-138	R15.5.5	this study	Turtle Rock middle	erratic	−75.3760	−111.3016	563	1.000	–
TUR-139	R15.5.6	this study	Turtle Rock middle	erratic	−75.3767	−111.3005	549	0.988	–
TUR-140	R15.5.7	this study	Turtle Rock middle	erratic	−75.3769	−111.3008	542	0.997	–
TUR-141	R15.5.8	this study	Turtle Rock middle	erratic	−75.3769	−111.3010	543	0.998	–
TUR-142	R15.5.9	this study	Turtle Rock middle	erratic	−75.3764	−111.3014	558	0.998	–
TUR-143	R15.5.10	this study	Turtle Rock middle	erratic	−75.3756	−111.2987	567	0.999	–
TUR-117	R15.3.17	this study	Turtle Rock low	erratic	−75.3811	−111.3066	451	0.999	–
TUR-132	R15.3.19	this study	Turtle Rock low	erratic	−75.3830	−111.3091	446	1.000	–
TUR-134	R15.3.21	this study	Turtle Rock low	erratic	−75.3839	−111.3149	444	1.000	–
TUR-135	R15.3.22	this study	Turtle Rock low	erratic	−75.3857	−111.3184	438	1.000	–
TUR-202	R15.4.2	this study	Turtle Rock intermediate	erratic	−75.3760	−111.2953	516	0.969	–
TUR-205	R15.4.5	this study	Turtle Rock intermediate	erratic	−75.3760	−111.2951	517	0.979	–
ICE-102	R15.10.2	this study	Icefall Nunatak	erratic	−75.3902	−111.2425	645	0.995	–
ICE-104	R15.9.4	this study	Icefall Nunatak	erratic	−75.3863	−111.2664	512	0.999	–
ICE-109	R15.9.9	this study	Icefall Nunatak	erratic	−75.3872	−111.2617	542	0.999	–
ICE-111	R15.9.11	this study	Icefall Nunatak	erratic	−75.3875	−111.2557	563	1.000	–
ICE-115	R15.11.1	this study	Icefall Nunatak	erratic	−75.3880	−111.2436	579	0.997	–
ICE-116	R15.11.2	this study	Icefall Nunatak	erratic	−75.3879	−111.2469	572	0.998	–
ICE-119	R15.10.5	this study	Icefall Nunatak	erratic	−75.3895	−111.2386	650	0.999	–
ICE-201	R15.9.1	this study	Icefall Nunatak	erratic	−75.3869	−111.2631	532	0.999	–
DOR-101	R15.18.1	this study	Dorrel Rock	erratic	−75.4446	−111.3687	694	1.000	–
DOR-102	R15.18.2	this study	Dorrel Rock	erratic	−75.4440	−111.3749	680	1.000	–
DOR-104	R15.18.4	this study	Dorrel Rock	erratic	−75.4447	−111.3665	685	0.997	–
DOR-106	R15.18.6	this study	Dorrel Rock	erratic	−75.4450	−111.3646	672	1.000	–
DOR-107	R15.18.7	this study	Dorrel Rock	erratic	−75.4456	−111.3620	650	0.990	–
DOR-108	R15.18.8	this study	Dorrel Rock	erratic	−75.4455	−111.3626	662	0.999	–
DOR-02	R9.4.2	2010	Dorrel Rock	erratic	−75.4445	−111.3678	699	1.000	–
NOT-101	R15.16.1	this study	Notebook Cliffs	erratic	−75.3931	−111.1393	834	0.994	–
NOT-103	R15.16.3	this study	Notebook Cliffs	erratic	−75.3914	−111.1398	852	0.998	–
NOT-104	R15.16.4	this study	Notebook Cliffs	erratic	−75.3886	−111.1175	893	0.998	–
NOT-107	R15.16.7	this study	Notebook Cliffs	erratic	−75.3882	−111.0906	885	0.998	–
MUY-02	R9.3.2	2010	Kay Peak ridge	erratic	−75.2208	−110.9599	338	1.000	–
MUY-05	R9.3.5	2010	Kay Peak ridge	bedrock	−75.2206	−110.9595	338	0.999	–
MUY-07	R9.3.7	2010	Kay Peak ridge	bedrock	−75.2207	−110.9591	334	0.994	–
MUY-08	R9.3.8	2010	Kay Peak ridge	erratic	−75.2205	−110.9612	326	0.942	–
MUY-10	R9.3.10	2010	Kay Peak ridge	erratic	−75.2206	−110.9611	324	0.977	–
MUY-11	R9.3.11	2010	Kay Peak ridge	erratic	−75.2205	−110.9608	327	0.941	–
KAY-101	R15.13.1	this study	Kay Peak ridge	bedrock	−75.2206	−110.9598	334	0.999	–
KAY-103	R15.13.3	this study	Kay Peak ridge	bedrock	−75.2196	−110.9591	302	0.997	–
KAY-105	R15.14.1	this study	Kay Peak ridge	bedrock	−75.2165	−110.9627	150	0.993	–
KAY-107	R15.14.3	this study	Kay Peak ridge	bedrock	−75.2167	−110.9629	160	0.996	–
KAY-108	R15.14.4	this study	Kay Peak ridge	bedrock	−75.2169	−110.9631	167	0.994	–
KAY-109	R15.14.5	this study	Kay Peak ridge	bedrock	−75.2170	−110.9632	170	0.997	–
KAY-110	R15.14.6	this study	Kay Peak ridge	bedrock	−75.2168	−110.9630	161	0.997	–
KAY-111	R15.14.7	this study	Kay Peak ridge	bedrock	−75.2166	−110.9628	154	0.994	–

processing software. Using this technique, position accuracy at the centimetre level was achieved without the need for running a separate GNSS receiver as a base station in the field. In order to determine how much thicker the ice sheet was when it deposited the erratics, the elevation of the modern ice surface was derived from a Digital Elevation Model (DEM). For DEM construction and post-processing of GPS measurements, see Supplementary Material.

Data on the geomorphological situation of the erratics (Supplementary Figs. S2-S5), their shape, roundness, long axis orientation, size and shielding (Table S1) and degree of weathering (Table S2) were recorded prior to sampling.

4.2. Analytical procedures and exposure age calculations

Samples were prepared for ^{10}Be measurement at Lamont-Doherty Earth Observatory cosmogenic nuclide laboratory (LDEO), and for in situ ^{14}C measurement at both LDEO (1 sample) and Tulane University Cosmogenic Nuclide Laboratory (8 samples). ^{10}Be analyses were undertaken at the Center for Accelerator Mass Spectrometry, Lawrence Livermore National Laboratory, USA (CAMS), and Scottish Universities Environmental Research Centre, UK. ^{14}C was measured at CAMS and Woods Hole National Ocean Sciences Accelerator Mass Spectrometry facility, USA. Details of all analytical procedures, exposure age calculations and analytical data are pro-

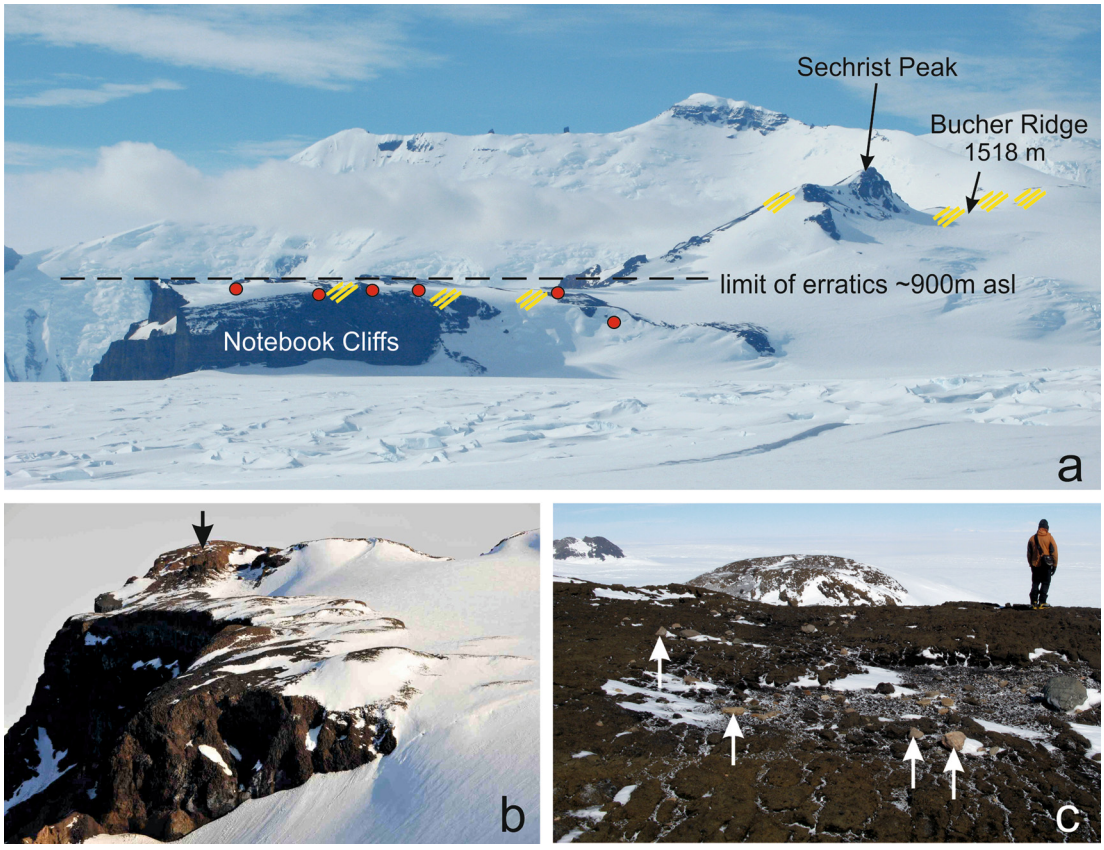

Fig. 3. The Icefall Nunatak-Notebook Cliffs-Bucher Ridge sequence. a. Notebook Cliffs, Sechrist Peak and Bucher Ridge viewed from the south-west. Erratics were not observed above 900 m asl, but striated bedrock surfaces (general locations indicated by diagonal yellow lines) are ubiquitous up to at least 1518 m asl on Bucher Ridge. b. Terraces on Icefall Nunatak, viewed from Turtle Rock looking SE. Field of view is 800 m; distance between nearest and furthest rock outcrops visible is 1250 m. Arrow shows location of image shown in panel c. c. The summit surface of Icefall Nunatak. Quartz-bearing erratics (indicated by arrows) are abundant, and perched on hyaloclastite breccia bedrock. Dorrel Rock is visible in the background (far left). Person for scale.

vided in Supplementary Material and Tables S3 and S4, and ^{10}Be data are publicly accessible at the UK Polar Data Centre (https://doi.org/10.5285/63bbaf4f-fe53-45a8-b2b5-d41adcf3d35f).

5. Results

5.1. Evidence for past ice cover

Evidence for former ice cover of the study sites is widespread. Almost all sites host erratic cobbles and boulders, and striated bedrock surfaces were observed on those where erratics are scarce or absent. The density of erratics across the study area was observed to decrease with increasing elevation. Three possible explanations for absence of erratics at higher elevations are: i) the LGM ice sheet did not thicken sufficiently to deposit erratics there; ii) the overriding ice sheet was not transporting enough material to deposit erratics there; and iii) erratics deposited during a previous ice-free period were removed by the LGM ice sheet as it flowed over the sites. Glacial-geological observations from each site are described below.

5.1.1. Turtle Rock

Four areas of Turtle Rock were examined for evidence of ice cover (Fig. 2a). Numerous erratic cobbles and boulders are scattered over all of these up to 685 m asl (i.e. within 30 m of the summit). Above this elevation, no erratics or striated bedrock surfaces were observed, although the friable lava surface would be unlikely to preserve striations. The presence of erratics with or without striated bedrock implies that Turtle Rock experienced ice cover at least up to 685 m asl at some time in the past. The lowermost terrace ("LOW" in Fig. 2a) hosts the greatest density of erratics so far reported from anywhere in the ASE, with a range of sizes between <20-180 cm diameter (Table S1) and several different lithologies (predominantly granite, granodiorite and gneiss; Table 1) (Fig. 2b). It is also the only site across the whole study area where metre-sized erratics were seen. The middle terrace ("MID" in Fig. 2a) consists of a gently sloping and undulating hyaloclastite bedrock surface, scattered with perched erratic cobbles of granite and granodiorite lithologies, and patches of till. Erratics observed on the higher slopes of Turtle Rock ("INT" and "HIGH" in Fig. 2a) were mostly <20 cm diameter and less strongly weathered than those at lower elevations. Striated surfaces were only observed in bedrock on the lowermost terrace. These were strongly striated in a N-S direction, parallel to the present flow direction of Pope Glacier.

5.1.2. Icefall Nunatak-Notebook Cliffs-Bucher Ridge

Notebook Cliffs comprises a broad basaltic platform at ~900 m asl (Fig. 3a) with near-vertical cliffs on its northern side. A few granitic erratics are strewn across the basalt bedrock surface where SSE-NNW-trending striations are also commonly-preserved. The erratics exhibit a moderate degree of weathering (Table S1), and there are notably many fewer than at Icefall Nunatak just below. At Icefall Nunatak a series of basalt terraces step up from 512 m to 575 m asl (Fig. 3b), with two rounded hyaloclastite knolls above (the highest is 659 m asl). All are covered with abundant erratic cobbles (Fig. 3c), providing evidence that ice has overridden the whole nunatak in the past. The erratics are mostly of

Fig. 4. Glacial features on Dorrel Rock and near Kay Peak. a. Streamlined shape of Dorrel Rock, looking westward. In the distance is Pope Glacier, flowing left to right. Person for scale. b. Abundant quartz-bearing erratic cobbles on Dorrel Rock. Compass for scale. c. Striated gneiss bedrock (pencil shows orientation) on a ridge extending northward between Kay Peak and the Crosson Ice Shelf.

small-medium size (i.e. <35 cm long axis), and of similar granitic lithologies to those found at Turtle Rock. However, they are not as abundant as those on the lower terrace of Turtle Rock; their spatial distribution and size is closer to erratics observed on the middle and intermediate terraces. At Bucher Ridge no erratics were observed (i.e. none above 893 m asl). Nevertheless, NW-SE-trending striations were found to be widespread on the bedrock surfaces, indicating that ice must have flowed over the ridge at some time in the past.

5.1.3. Dorrel Rock

This nunatak has both a rounded roche mountonée shape (Fig. 4a) and heavily striated upper surface, consistent with erosion and moulding by ice. Numerous erratic cobbles and pebbles of granitic lithology – the most abundant of all sites visited for this study – are perched on the gabbroic bedrock (Fig. 4b). The majority of cobbles at this site are sub-rounded or rounded and have the lowest degree of weathering of all the sites visited (Table S1), implying extensive erosion during relatively-recent glacial transport.

5.1.4. Kay Peak ridge

Very few glacially-deposited exotic erratics were observed at this site, but the bedrock is strongly striated, indicating that ice flowed over it in the past (Fig. 4c). Two sets of striations exist: E-W-oriented striations correspond with the present flow direction of Pope Glacier around the foot of the ridge and out into Crosson Ice Shelf (Fig. 1b), while others that are N-S-oriented reflect the present flow direction of the main trunk of Pope Glacier.

5.2. ^{10}Be and in situ ^{14}C exposure ages

^{10}Be exposure ages were obtained from 44 erratics and five bedrock samples. In situ ^{14}C ages were also obtained from four of these (one erratic, three bedrock). Five bedrock samples were analysed for in situ ^{14}C only. The majority of ^{10}Be and ^{14}C ages are in the range 5.5-16 ka, and all except four are older than 5 ka (Fig. 5; all uncertainties are reported as 1σ external errors). All ages postdate the Last Glacial Maximum (LGM), and are reported assuming no snow cover (see Supplementary Material for explanation). Three published ^{10}Be ages from erratics from Turtle Rock (TR1, TR2 and TR3; Johnson et al., 2008) are consistent with the new data, and will also be included in the discussion. Whilst the range of bedrock and erratic ^{10}Be ages overlap (Fig. 5), the oldest two bedrock exposure ages are the oldest reported from the ASE thus far. This difference implies that the bedrock contains ^{10}Be inherited from prior exposure (e.g. Stone et al., 2003 and Johnson et al., 2017), and it follows that the other bedrock ages in this area may be similarly affected. Thus, in this area, ^{10}Be ages on erratics are likely to be more reliable as deglaciation ages than ^{10}Be ages from bedrock.

Some of the exposure ages from the nunataks surrounding Mt Murphy form a trend of decreasing age with decreasing altitude, which we interpret as recording progressive lowering of the ice sheet surface. For example, ages from Icefall Nunatak range from 7.9-6.9 ka in a well-constrained profile over an altitudinal range of 138 m (Fig. 5). In contrast, however, the range of exposure ages from Turtle Rock is much greater (21.3-5.9 ka), with different ages frequently obtained from samples at any given altitude (Fig. 5), especially on the high, middle and intermediate terraces. In situ ^{14}C dating was undertaken on one sample to verify the timing of deglaciation at that elevation, and therefore to determine whether ^{10}Be inheritance is causing the spread of ^{10}Be ages on the upper terraces of Turtle Rock. Due to its short half-life, in situ ^{14}C decays rapidly during ice cover, hence its abundance in a rock surface reflects the ^{14}C accumulated only since the LGM. This method therefore provides a more reliable date for the last deglaciation in areas where ^{10}Be inheritance is prevalent. The resulting age (9.9 $\pm$ 0.9 ka; from sample TUR-138) is identical within error to the ^{10}Be age on the same sample (10.2 $\pm$ 0.7 ka; Fig. 5). This indicates that the middle terrace deglaciated around 10 ka, implying a) that samples with older ^{10}Be ages from this elevation are affected by ^{10}Be inheritance, and b) that since the ^{10}Be age of 5.9 $\pm$ 0.4 ka from TUR-118 is younger than the timing of deglaciation, it must reflect a post-depositional process not experienced by all samples at this elevation (e.g. rolling). The latter could also be an explanation for the two ^{10}Be ages that are <5 ka (TUR-127 and NOT-101; Fig. 5): Persistent shielding by snow for several months each year would result in apparent exposure ages being younger than the timing of deglaciation. However, applying a correction for snow cover to those samples would not bring them in line with other ages from Turtle Rock and Notebook Cliffs. The ages for TUR-127, NOT-101 and TUR-118 are therefore excluded from further discussion.

At Notebook Cliffs and Dorrel Rock, exposure ages are clustered together around 9 ka and 8-6 ka respectively (Fig. 5). Although the samples were not collected over sufficient altitudinal range to record a lowering trend, they extend the profile from Icefall Nunatak approximately 250 m higher. At the lower end of the sequence, along Kay Peak ridge, samples extend the ice surface lowering profile a further 288 m below that recorded by the lower Turtle Rock samples. ^{10}Be exposure ages for three erratic cobbles range from 9.9-15.1 ka at ~330 m asl (Fig. 5). With the exception of one sample, bedrock ^{10}Be ages are all >20 ka. In contrast, in situ ^{14}C ages for bedrock samples from 150-334 m altitude are all much younger, with Holocene ages (3.7-8.0 ka; Fig. 5). This difference suggests ^{10}Be inheritance is ubiquitous in these samples, and implies that the ^{14}C ages are therefore more reliable as deglaciation ages at this site.

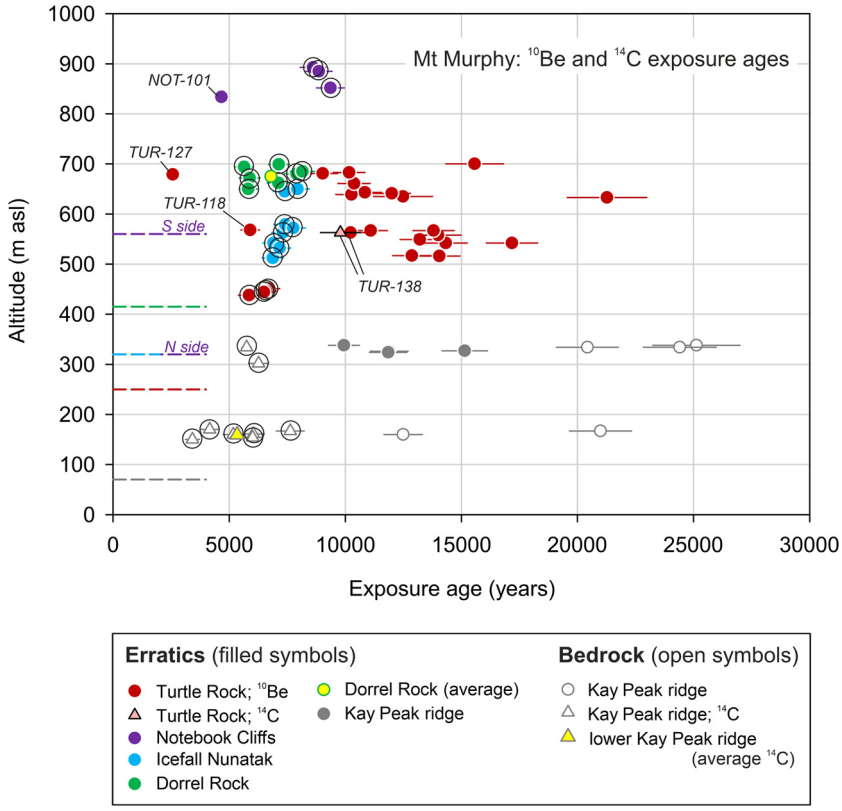

Fig. 5. Exposure age versus altitude for samples from Mt Murphy and surrounding nunataks; in addition to results from the present study, three pre-existing ages from Turtle Rock are included (see text). All uncertainties are reported as 1σ external errors. Circled samples are those used for the linear regression analysis (section 6.2 and Fig. 7). Dashed lines show modern ice surface elevations adjacent to each study site, as indicated by the colour.

6. Discussion

6.1. Constraints on the extent and timing of thinning since the LGM

To interpret the range of exposure ages determined from the nunataks surrounding Mt Murphy, we consider the relative locations of each sample site in relation to Pope Glacier (Fig. 6). Erratics collected from sites that are oriented perpendicular to ice flow are most likely to record a reliable signature of the last episode of deglaciation because they would be swept off the nunatak ridges by any subsequent glaciations. Therefore, exposure ages from nunataks forming the Notebook Cliffs-Icefall Nunatak-Bucher Ridge sequence are expected to provide a profile of surface lowering of Pope Glacier with time that is not complicated by ^{10}Be inheritance. Since the lower Turtle Rock site also extends westward from the Notebook Cliffs-Icefall Nunatak-Bucher Ridge sequence towards Pope Glacier, exposure ages derived from there would further extend this profile.

Fig. 6 provides a visual representation of the timing and magnitude of surface lowering at these sites. The cluster of ages from Notebook Cliffs implies that the ice sheet surface was at or above 893 m asl at 9 ka. No deglaciation ages were obtained from higher than this – i.e. from Bucher Ridge – because the basaltic bedrock lithology is not suitable for ^{10}Be dating, and erratics are absent; hence we do not have any evidence for ice sheet thickness above 893 m asl, and consequently no additional constraints on the maximum LGM ice sheet thickness in the ASE. The ^{10}Be exposure age data from Icefall Nunatak and lower Turtle Rock indicate that the ice surface lowered steadily by 212 m between 7.9-5.9 ka (Figs. 5 and 6).

Interpretation of exposure age data from the remaining sample sites – Dorrel Rock, the high, middle and intermediate terraces of Turtle Rock (Fig. 2), and Kay Peak ridge – is more complicated. Dorrel Rock is located at the confluence of Pope Glacier and one of its tributaries (Fig. 1b). Exposure age data from there could be interpreted as recording deglaciation of either Pope Glacier or the tributary glacier. However, since thinning of ice at the grounding line of Pope Glacier would likely propagate upstream (cf. Jamieson et al., 2012), changes in surface lowering detected on the tributary should reflect lowering of Pope Glacier itself. Samples from Dorrel Rock were collected over a relatively small altitudinal range (50 m), thus the average exposure age from that site (6.8 ± 1.0 ka; mean and standard deviation) provides the best estimate of the timing for its deglaciation and concurs with the timing of deglaciation of Notebook Cliffs, Icefall Nunatak, and the lower terrace of Turtle Rock (Fig. 5).

In situ ^{14}C dating provides insight into why some of the ^{10}Be ages from the upper, middle and intermediate terraces of Turtle Rock are either too young or too old to represent the timing of deglaciation. The ^{14}C age for TUR-138 implies that the middle terrace of Turtle Rock deglaciated earlier (~10 ka; section 5.2) than the other study sites, even though the site is lower than some (e.g. Notebook Cliffs). A plausible explanation for this relates to the presence of a windscoop around the base of Turtle Rock (Fig. 2a), which, if present during deglaciation, would have resulted in a consistently lower ice surface on the downstream side of Turtle Rock (near the middle terrace) than on the upstream side near Icefall Nunatak, Dorrel Rock and Notebook Cliffs. A second possibility is a situation whereby the tributary glacier responded to grounding line change later than Pope Glacier, resulting in deglaciation of Icefall Nunatak and Notebook Cliffs later than some lower sites on Turtle Rock. However, without more extensive in situ ^{14}C dating, it is difficult to verify either of these suggestions. The in situ ^{14}C dating also implies that ^{10}Be inheritance is prevalent in erratics from the high, middle and intermediate terraces of Turtle Rock, resulting in a range of older ^{10}Be ages that are unlikely

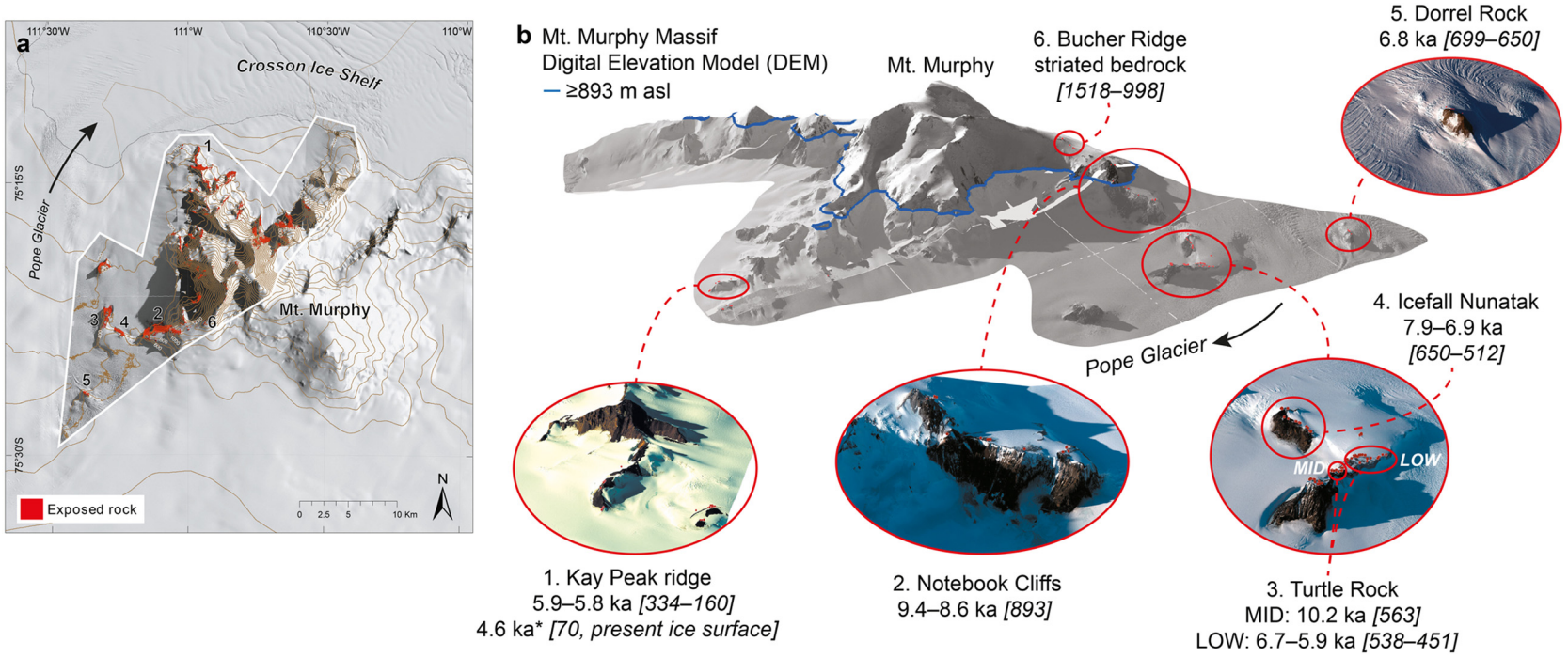

Fig. 6. Timing and magnitude of ice sheet thinning at Mt Murphy and surrounding nunataks. a. Map shows location of satellite imagery used to create the Orthorectified Digital Elevation Model (DEM; area inside white line), and positions of nunataks shown in panel b. Areas of exposed rock are derived from semi-automated bedrock mapping (see Supplementary Material). b. DEM with ranges of deglaciation ages for each site and their corresponding altitudes (metres above sea level, in italics). *Age derived from regression analysis (section 6.2). The inferred minimum ice sheet thickness at 10 ka is represented by the blue line and shading. Image: DigitalGlobe Products; WorldView-2 © 2013 and 2014 DigitalGlobe, Inc., a Maxar company.

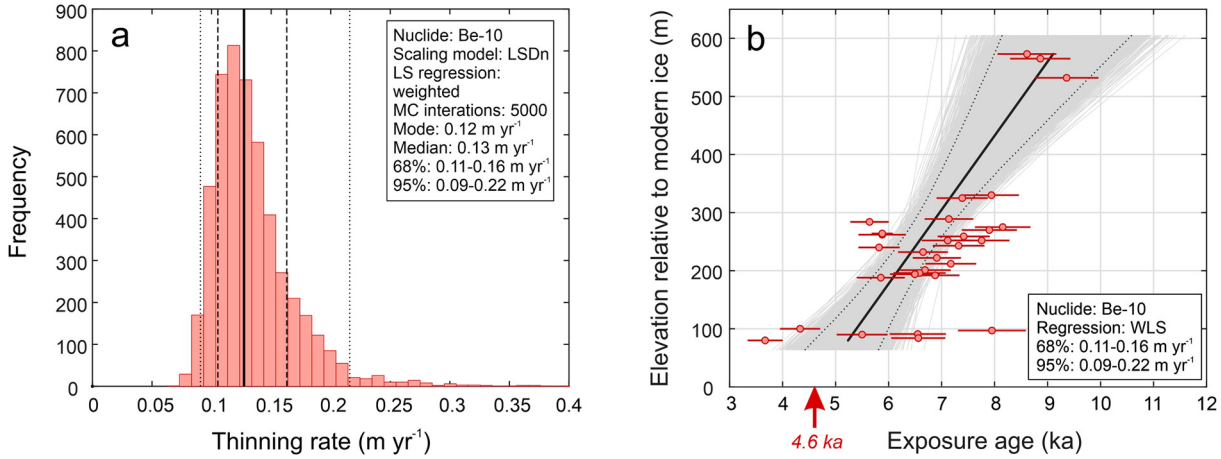

Fig. 7. Results of linear regression analysis to determine a best-fit profile of surface lowering of Pope Glacier during the Holocene. The exposure ages used for the analysis are those that are circled in Fig. 5 (data in Table S5). a) Histogram of modelled thinning rates showing 68% and 95% confidence intervals (dashed and dotted vertical lines, respectively). The best-fit rate is indicated by the solid black vertical line. b) Profile of ice surface lowering with time. Exposure ages are shown with 1σ external errors, and are plotted relative to the modern ice surface elevation (see Fig. 5). Grey lines represent all model fits to the data. The solid black line is the best-fit to the data, and dotted black lines represent the 95% confidence interval. The red arrow shows the timing of ice surface lowering to its modern elevation.

to represent the timing of deglaciation. The altitudinal range of those samples (516-700 m asl) also overlaps with the range of the lower Turtle-Notebook Cliffs-Icefall Nunatak samples (438-893 m asl), so they provide no additional evidence for the pattern or timing of thinning of Pope Glacier. Consequently, the Icefall Nunatak ages provide the most reliable trajectory of ice surface lowering of Pope Glacier between 500 and 650 m asl (equivalent to 120-330 m above the modern ice sheet surface; Fig. 5).

In situ ^{14}C exposure ages from Kay Peak ridge bedrock imply that, during the Holocene, the ice surface lowered to within 80 m of its modern elevation (Figs. 5 and 6). However, the timing of deglaciation of the lowest presently-exposed surfaces of the ridge is not clear because ages there span a period of several thousand years (3.7 $\pm$ 0.3 to 8.0 $\pm$ 0.6 ka; KAY-105 to KAY-111). This range may be due to curvature of the ridge crest and the consequent complexity of snow/ice cover: variation in sample locations relative to the crest could have resulted in some samples being exposed earlier than others from the same elevation. Although there is no systematic variation of exposure age with distance from ridge crest, this cannot be ruled out. Therefore the average ^{14}C exposure age (5.8 $\pm$ 1.4 ka; mean and standard deviation; Fig. 5) provides a best estimate for timing of deglaciation of the lower part of Kay Peak ridge.

6.2. Determining a "best-fit" thinning profile for Pope Glacier

A Monte Carlo linear regression analysis using the MATLAB® model "iceTEA" (http://ice-tea.org; Jones et al., 2019) was used to determine the profile of ice surface lowering that best fits the exposure age data. Rates of lowering were generated from 5000 iterations through randomly-sampled points using 2σ internal uncertainties. Prior to analysis, exposure ages from samples that are unlikely to represent timing of deglaciation for one of the following reasons were removed: i) they are not the youngest ^{10}Be exposure age at a given elevation, implying ^{10}Be inheritance, ii) they are anomalously young (>2 standard deviations from the mean), and to the authors' knowledge there is no plausible geomorphological explanation that would be consistent with their exposure age(s) representing deglaciation, and iii) they are from the middle, intermediate or upper terraces of Turtle Rock which may have been influenced by presence of a windscoop throughout the last deglaciation. A modelled thinning rate range, best-fit thinning rate and profile are produced by the analysis. The thinning rate for Mt Murphy ranges from 0.11-0.16 m yr^{-1} (1σ; 68 %) and 0.09-0.22 m yr^{-1} (2σ; 95 %), and the best-fit rate is 0.13 m yr^{-1} (Fig. 7). Extrapolation of the best-fit line to the modern surface elevation of Pope Glacier suggests that the ice surface had lowered to that elevation by 4.6 ka (Fig. 7b). The implications of this analysis are discussed in section 6.3.

6.3. Comparison with existing records of Holocene ice sheet change in the ASE

The exposure age data presented here indicate a sustained period of several hundred metres of ice surface lowering during the early- to mid-Holocene, 9-6 ka. Exposure dating studies from three other coastal sites in the central and eastern ASE have provided evidence for deglaciation contemporaneous with this: when calculated using the same scaling and ^{10}Be production rate, Barter Bluff at 735 m asl in the Kohler Range was deglaciated by 8.7 ka (Lindow et al., 2014) and Hunt Bluff at 470 m asl on the western side of Bear Peninsula was deglaciated by 9.6 ka (Johnson et al., 2017) (Fig. 8). Furthermore, exposure ages from samples situated at 187-366 m asl at two peaks in the Hudson Mountains, adjacent to Pine Island Glacier, together document a period of abrupt thinning resulting in at least 142 m of lowering around 7 ka (Johnson et al., 2014). Thus deglaciation during the early Holocene appears to have been widespread in the ASE.

In contrast to the timing of deglaciation, it is more difficult to compare the magnitude of surface lowering detected at Mt Murphy (≥560 m) with sites across the wider ASE because existing thinning profiles do not cover as wide an altitudinal range. For example, the results from the Kohler Range and Bear Peninsula were obtained from flat-topped bluffs edged by near-vertical cliffs, where altitudinal range of more than a few metres is difficult to sample. In the Hudson Mountains, at least 142 m of lowering has been detected, but exposure dating of the upper parts of the highest peaks in the range (which rise to 835 m asl) has not been undertaken, so it is not yet possible to determine if surface lowering was as extensive in the eastern ASE as it was in the central ASE. Furthermore, evidence of the maximum LGM ice sheet thickness in the region remains undetermined. The highest site dated at Mt Murphy (Notebook Cliffs at 893 m asl) is the highest of all the sites in the ASE dated so far, but the present study suggests that it has been exposed only since ~9 ka. Constraints on the maximum LGM ice surface height can only be obtained by exposure dating of samples from higher elevations of Mt Murphy (the only

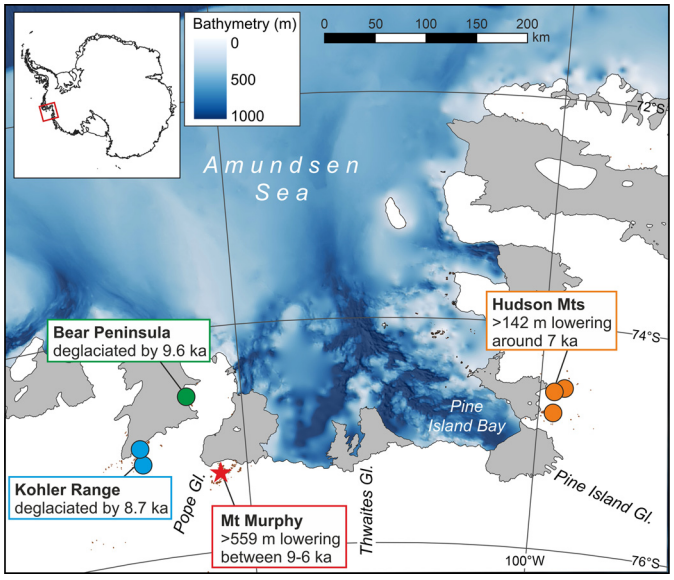

Fig. 8. Summary of current knowledge of terrestrial ice sheet change across the ASE in the Holocene. Locations of sites where studies have been undertaken are shown: Mt Murphy (Johnson et al., 2008 and this study); Kohler Range (Lindow et al., 2014); Bear Peninsula (Johnson et al., 2017); Hudson Mountains (Johnson et al., 2014). Bathymetry is from the International Bathymetric Chart of the Southern Ocean (Arndt et al., 2013).

higher peak in the region is Mt Takahe, which is almost entirely snow-covered).

The best-fit rate of thinning of Pope Glacier determined from the present study is 0.13 ± 0.09/0.04 m yr^{-1} (Fig. 7b). This is towards the lower end of the range of thinning rates from across all of Antarctica determined using the same approach (0.02-1.67 m yr^{-1}; Small et al., 2019, Table 3). The only other place in the ASE where the altitudinal range of existing dated samples is sufficient to determine thinning rate is the Hudson Mountains, adjacent to Pine Island Glacier (Fig. 8; Johnson et al., 2014). In comparison with Pope Glacier, much higher average rates of thinning were determined by Small et al. (2019) for two nunataks there – 1.16 and 1.67 m yr^{-1} for Maish Nunatak and Mt Moses, respectively – despite their similar setting (both Pope Glacier and Pine Island Glacier drain the Pine Island-Thwaites catchment, and were formerly connected, as evidenced by palaeo-ice stream troughs that coalesce on the mid-continental shelf; Fig. 8). The relatively lower thinning rate derived for Pope Glacier from the present study could be interpreted as implying that, during the early Holocene, the response of Pope Glacier and Pine Island Glacier to environmental change (e.g. incursion of warm Circumpolar Deep Water at their grounding lines, as is the case today; Hillenbrand et al., 2017; Scheuchl et al., 2016) was not the same, i.e. that Pine Island Glacier responded more abruptly than Pope Glacier. Alternatively, it could imply that the glaciers were not both subjected to the same external forcing. In contrast to the Hudson Mountains where samples were dated right down to the modern ice surface (Johnson et al., 2014), at Mt Murphy, the lowest samples collected are from 80 m above the ice surface (on Kay Peak ridge). Whilst these broadly constrain the timing of deglaciation to the Holocene epoch, due to their scatter, a more precise timing is best estimated from the average exposure age of those samples (5.8 ± 1.4 ka). The regression analysis suggests that the ice surface lowered further, to its present elevation, during the mid-Holocene (by 4.6 ka; Fig. 7b). Thus, the exposure age data are consistent with a steady rate of thinning of Pope Glacier from the early- to mid-Holocene. However, since there is a lack of data between 230 and 100 m above the modern ice sheet surface and over the lowest 80 m (Fig. 7b), we cannot preclude a scenario whereby the glacier underwent one or more episodes of faster thinning during the mid- to late-Holocene. Consequently, it is not yet possible to make a direct comparison between the thinning rates of Pine Island Glacier and Pope Glacier. Nevertheless, several hundreds of metres of ice surface lowering within a few thousand years – or centuries in the case of Pine Island Glacier – in the early- to mid-Holocene implies a strong forcing acting at both sites simultaneously.

6.4. Palaeoclimatic context for Holocene thinning

Rapid thinning of Pope Glacier between 9 and 6 ka as documented by the exposure age data appears to have occurred at the same time as, or shortly after, global and regional climatic and oceanic changes that might have helped trigger ice sheet thinning in the ASE (Fig. 9). For example, although global mean sea level was still several tens of metres below present during early-to-mid Holocene (Lambeck et al., 2014), glacial isostatic adjustment (GIA) modelling suggests that water depths offshore from Pope Glacier were greater than present during this time. In particular, a highstand is predicted, with water depths estimated to have been up to 90 m greater than present, around 12 ka (Fig. 9a; Whitehouse et al., 2012; Argus et al., 2014; Peltier et al., 2015). Large uncertainties on those predictions mean that small localised changes in relative sea level (RSL) cannot be ruled out. Nevertheless, if correct, a local sea level highstand around 12 ka could have encouraged faster grounding line retreat in the early Holocene, resulting in an increased rate of ice sheet thinning shortly after.

As well as local changes in RSL, transport of warm ocean water onto the continental shelf in front of Pope Glacier was occurring during the early part of the Holocene: From modelling, ocean temperatures in the central ASE are predicted to have been rising sharply between ~11.5-4 ka (Liu et al., 2009; Fig. 9b), and in addition, proxies for Circumpolar Deep Water (CDW) advection from foraminifera in marine sediment cores suggest that there was increased upwelling of warm water onto the ASE shelf at a similar time (between 10.4-7.5 kyr BP, and possibly earlier; Fig. 3a-c, Hillenbrand et al., 2017). Geochemical proxies for the relative strength of Southern Hemisphere westerly winds, that could have enhanced upwelling of that CDW, show that they intensified in the SW Pacific sector of the Southern Ocean between 9.2-5.3 ka (Fig. 9c; Saunders et al., 2018). In contrast, atmospheric changes occurring inland, upstream from Pope Glacier at the WAIS Divide ice core site, indicate that no large-scale changes occurred there during the early Holocene: accumulation rate increased steadily throughout the Holocene, whilst atmospheric temperature was relatively stable (Fig. 9d; Cuffey et al., 2016; Fudge et al., 2016). Therefore, it appears that the ocean had a stronger influence on the extensive thinning of Pope Glacier during the early Holocene than atmospheric or climatic changes. The timing of deglaciation appears to support that interpretation.

Although external oceanic forcings such as ocean temperatures and sea level in the early Holocene may have accelerated grounding line retreat of Pope Glacier causing upstream thinning, a reduction in buttressing by an ice shelf could also have been a trigger. If such an ice shelf extended across the central and eastern ASE, any weakening of that ice shelf would be expected to affect both Pope Glacier and Pine Island Glacier simultaneously. The deglacial history determined for Mt Murphy by the present study and for the Hudson Mountains – adjacent to Pine Island Glacier – by Johnson et al. (2014) imply several hundred metres of thinning at both sites during the early- to mid-Holocene. This is consistent with evidence from a marine sediment core from the middle continental shelf SW of Burke Island for loss of an ice shelf that spanned the ASE from ~12.3-10.6 cal kyr BP (Fig. 8, Kirshner et al., 2012). High rates of CDW upwelling onto the continental shelf during the early Holocene are thought to have provided a mechanism for that ice

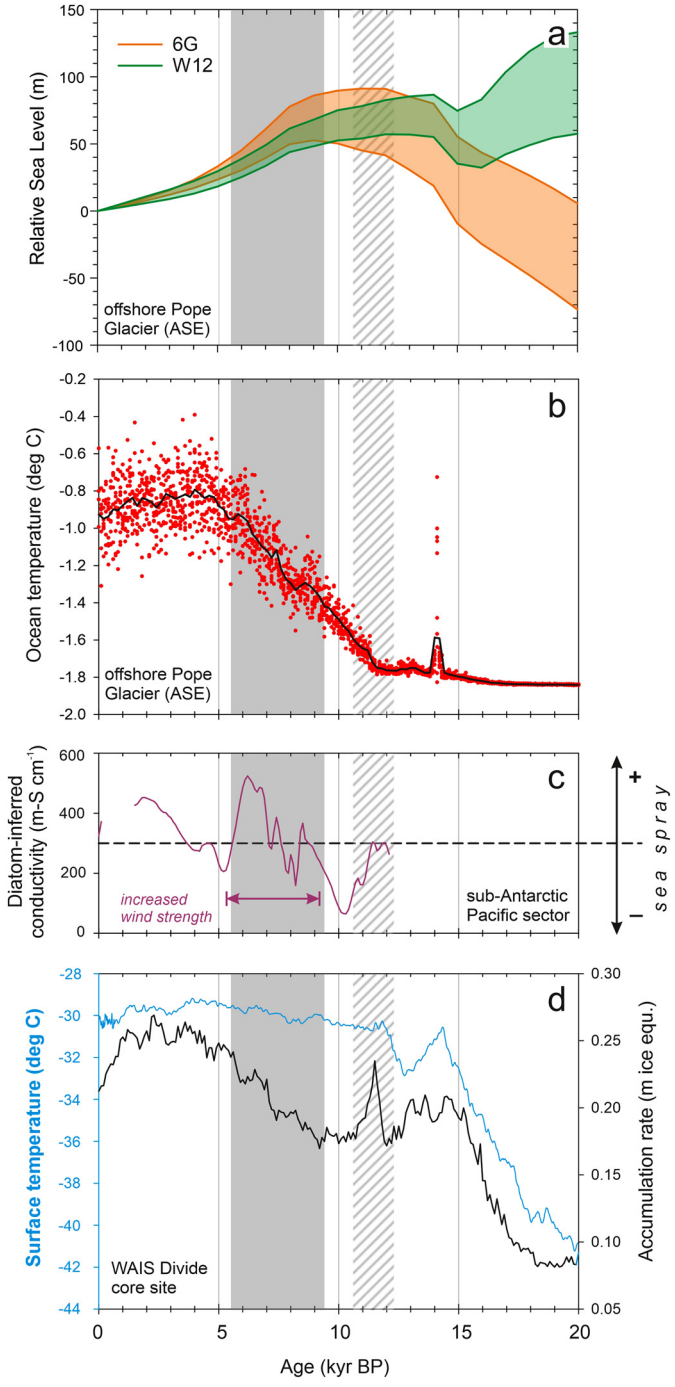

Fig. 9. Palaeoclimatic context for Holocene thinning of Pope Glacier. Grey shaded area denotes the period of deglaciation of Mt Murphy determined from exposure dating (~9-6 ka; this study), and diagonally-hashed area indicates presence of an ice shelf across the central and eastern ASE (12.3-10.6 cal kyr BP; Kirshner et al., 2012). Datasets are: (a) Relative sea level change 150 km offshore from Pope Glacier – at 74°S / 108°W – derived from GIA modelling (Whitehouse et al., 2012; Argus et al., 2014; Peltier et al., 2015). Predictions are for the ICE-6G_C and W12 ice history models; the shaded regions reflect the range of model predictions for a suite of 10 Earth models (lithosphere thickness varies from 71-120 km, upper mantle viscosity varies from 0.3-1.0 $\times 10^{21}$ Pa s, and lower mantle viscosity is 10^{22} Pa s).; (b) Modelled ocean temperature at 400 m water depth in the central ASE (Liu et al., 2009; data were extracted for the location 73.435°S / 108.700°W) – 400 m depth was selected because this is the typical depth where CDW is located. (c) Proxy for strength of Southern Hemisphere westerly winds that track input of sea-salt aerosols (diatom-inferred conductivity, measured in a lake sediment core from sub-Antarctic Macquarie Island; Saunders et al., 2018). Pink arrow indicates a period of increased wind strength in the early- to mid-Holocene, 9.2-5.3 ka.; (d) Atmospheric temperature (blue line; Cuffey et al., 2016) and accumulation at WAIS Divide core site (black line; Fudge et al., 2016).

shelf loss (Hillenbrand et al., 2017). It is therefore plausible that loss of this more extensive ice shelf that buttressed the flow of both Pope Glacier and Pine Island Glacier (and presumably also therefore, flow of Thwaites Glacier in between), facilitated by enhanced CDW upwelling, was the trigger for several hundred metres of grounded ice thinning across a broad area of the ASE. However, there is also evidence that a smaller ice shelf was maintained in Pine Island Bay until 7.5 cal kyr BP (Hillenbrand et al., 2017), so debuttressing of Pope and Pine Island Glaciers could have been a stepwise process. The role of oceanic forcing and ice shelf buttressing in ice sheet thinning could be tested with ice sheet modelling.

7. Conclusions and suggestions for future work

This study investigates the timing and extent of surface lowering of Pope Glacier since the LGM. From a new dataset of cosmogenic ^{10}Be measurements, the following conclusions are drawn:

1. Exposure ages from erratic cobbles and bedrock collected from Mt Murphy and surrounding nunataks are predominantly in the range 5.5-16 ka.
2. Pope Glacier experienced 560 m of surface lowering in the early- to mid-Holocene (9-6 ka) at a rate of 0.13 ± 0.09/0.04 m yr^{-1}. This is much lower than the rate of early Holocene thinning of Pine Island Glacier in the eastern ASE (>1.0 m yr^{-1}; Johnson et al., 2014) but the data do not preclude one or more episodes of faster thinning over the last ~200 metres above the modern ice surface.
3. Reduction in buttressing by an ice shelf that covered the mid-inner ASE shelf (cf. Kirshner et al., 2012) could have triggered the early Holocene thinning of Pope Glacier. Enhanced upwelling of warm CDW onto the inner continental shelf of the ASE (Hillenbrand et al., 2017), plus a potential early Holocene peak in local sea level, are likely to have facilitated this.
4. At 9 ka, the ice sheet surface was situated at or above 893 m above modern sea level. Striated bedrock surfaces observed up to 1518 m asl suggest that the maximum thickness of the ice sheet at LGM may have been higher, but this hypothesis remains to be tested.

The rates of thinning of Pope Glacier prior to 9 ka and in the late Holocene are not yet known, but are needed to constrain ice sheet and GIA models, respectively. Therefore future work should include:

- Subglacial bedrock recovery drilling to determine whether the ice sheet surface was ever below present during the late Holocene (which would imply a retreat–re-advance cycle).
- Dating of basaltic bedrock samples collected from elevations above those analysed for this study, to determine whether the ice sheet surface was higher than 893 m at the LGM.
- Model experiments to test potential triggers for widespread early Holocene thinning in the ASE.

CRediT authorship contribution statement

Joanne S. Johnson: Conceptualization, Funding acquisition, Investigation, Methodology, Project administration, Supervision, Visualization, Writing - original draft. **Stephen J. Roberts:** Conceptualization, Funding acquisition, Investigation, Methodology, Visualization, Writing - review & editing. **Dylan H. Rood:** Conceptualization, Funding acquisition, Investigation, Methodology, Supervision, Writing - review & editing. **David Pollard:** Conceptualization, Investigation, Writing - review & editing. **Joerg M. Schaefer:** Conceptualization, Methodology, Supervision, Writing - review & editing. **Pippa L. Whitehouse:** Conceptualization, Investigation, Writing -

review & editing. **Louise C. Ireland:** Methodology, Writing - review & editing. **Jennifer L. Lamp:** Investigation, Writing - review & editing. **Brent M. Goehring:** Methodology, Supervision, Writing - review & editing. **Cari Rand:** Investigation, Writing - review & editing. **James A. Smith:** Methodology, Writing - review & editing.

Declaration of competing interest

The authors declare that they have no known competing financial interests or personal relationships that could have appeared to influence the work reported in this paper.

Acknowledgements

We are grateful to British Antarctic Survey (BAS) Operations and Air Unit, and all staff at Rothera Research Station who made the fieldwork possible, especially field guides Alistair Docherty and Iain Rudkin whose professionalism and skill in the field were exemplary. John Smellie and Wes LeMasurier kindly provided information on sampling sites around Mt Murphy from their earlier field observations, and Hilary Blagbrough and Laura Gerrish (BAS), Jean Hanley (LDEO), Roseanne Schwartz (LDEO) and Sheng Xu (SUERC) provided technical support. Richard Selwyn Jones (Durham University) advised on data analysis for Fig. 7. The work has benefited from numerous conversations and collaborations with colleagues over the past decade, especially Claus-Dieter Hillenbrand, Richard Hindmarsh, Rob Larter and David Vaughan at BAS, John Smellie (University of Leicester), and Mike Bentley (Durham University). Some of the samples from Kay Peak ridge were collected in 2010 (see Table 1) whilst James Smith was on board RV *Polarstern* cruise ANT-XXVII-3. We acknowledge the support of Natural Environment Research Council (NERC) grants NE/K012088/1, NE/K011278/1 and NE/M013081/1. This work forms part of the British Antarctic Survey 'Polar Science for Planet Earth' programme, also funded by NERC. We are grateful for constructive comments from two anonymous reviewers that helped improve the manuscript.

Appendix A. Supplementary material

Supplementary material related to this article can be found online at https://doi.org/10.1016/j.epsl.2020.116501.

References

Ackert, R.P., Mukhopadhyay, S., Pollard, D., DeConto, R.M., Putnam, A.E., Borns, H.W., 2011. West Antarctic Ice Sheet elevations in the Ohio Range: geologic constraints and ice sheet modeling prior to the last highstand. Earth Planet. Sci. Lett. 307, 83–93.

Argus, D.F., Peltier, W.R., Drummond, R., Moore, A.W., 2014. The Antarctica component of postglacial rebound model ICE-6G_C (VM5a) based on GPS positioning, exposure age dating of ice thicknesses, and relative sea level histories. Geophys. J. Int. 198 (1), 537–563.

Arndt, J.E., Schenke, H.W., Jakobsson, M., Nitsche, F.O., Buys, G., Goleby, B., Rebesco, M., Bohoyo, F., Hong, J., Black, J., Greku, R., Udintsev, G., Barrios, F., Reynoso-Peralta, W., Taisei, M., Wigley, R., 2013. The International Bathymetric Chart of the Southern Ocean (IBCSO) Version 1.0—a new bathymetric compilation covering circum-Antarctic waters. Geophys. Res. Lett. 40, 3111–3117.

Balco, G., 2011. Contributions and unrealized potential contributions of cosmogenic-nuclide exposure dating to glacier chronology, 1990-2010. Quat. Sci. Rev. 30, 3–27.

Briggs, R.D., Tarasov, L., 2013. How to evaluate model-derived deglaciation chronologies: a case study using Antarctica. Quat. Sci. Rev. 63, 109–127.

Cuffey, K.M., Clow, G.D., Steig, E.J., Buizert, C., Fudge, T.J., Koutnik, M., Waddington, E.D., Alley, R.B., Severinghaus, J.P., 2016. Deglacial temperature history of West Antarctica. Proc. Natl. Acad. Sci. USA 113 (50), 14249–14254. https://doi.org/10.1073/pnas.1609132113.

Favier, L., Durand, G., Cornford, S.L., Gudmundsson, G.H., Gagliardini, O., Gillet-Chaulet, F., Zwinger, R., Payne, A.K., LeBrocq, A.M., 2014. Retreat of Pine Island Glacier controlled by marine ice-sheet instability. Nat. Clim. Change 117–121.

Fudge, T.J., Markle, B.R., Cuffey, K.M., Buizert, C., Taylor, K.C., Steig, E.J., Waddington, E.D., Conway, H., Koutnik, M., 2016. Variable relationship between accumulation and temperature in West Antarctica for the past 31,000 years. Geophys. Res. Lett. 43, 3795–3803. https://doi.org/10.1002/2016GL068356.

Hillenbrand, C.-D., Smith, J.A., Hoddell, D.A., Greaves, M., Poole, C.R., Kender, S., Williams, M., Andersen, T.J., Jernas, P.E., Elderfield, H., Klages, J., Roberts, S.J., Gohl, K., Larter, R.D., Kuhn, G., 2017. West Antarctic Ice Sheet retreat driven by Holocene warm water incursions. Nature 547, 43–48.

Jamieson, S.S.R., Vieli, A., Livingstone, S.J., Ó Cofaigh, C., Stokes, C., Hillenbrand, C.D., Dowdeswell, J.A., 2012. Ice-stream stability on a reverse bed slope. Nat. Geosci. 5, 799–802.

Jenkins, A., Dutrieux, P., Jacobs, S., Steig, E.J., Gudmundsson, G.H., Smith, J., Heywood, K.J., 2016. Decadal ocean forcing and Antarctic ice sheet response: lessons from the Amundsen Sea. Oceanography 29 (4), 106–117. https://doi.org/10.5670/oceanog.2016.103.

Johnson, J.S., Bentley, M.J., Gohl, K., 2008. First exposure ages from the Amundsen Sea Embayment, West Antarctica: the Late Quaternary context for recent thinning of Pine Island, Smith, and Pope Glaciers. Geology 36 (3), 223–226.

Johnson, J.S., Bentley, M.J., Smith, J.A., Finkel, R.C., Rood, D.H., Gohl, K., Balco, G., Larter, R.D., Schaefer, J.M., 2014. Rapid thinning of Pine Island Glacier in the early Holocene. Science 343, 999–1001.

Johnson, J.S., Smith, J.A., Schaefer, J.M., Young, N.E., Goehring, B.M., Hillenbrand, C.-D., Lamp, J.L., Finkel, R.C., Gohl, K., 2017. The last glaciation of Bear Peninsula, central Amundsen Sea Embayment of Antarctica: constraints on timing and duration revealed by in situ cosmogenic ^{14}C and ^{10}Be dating. Quat. Sci. Rev. 178, 77–88.

Jones, R.S., Small, D., Cahill, N., Bentley, M.J., Whitehouse, P.L., 2019. Tools for plotting and analysing cosmogenic-nuclide surface-exposure data from former ice margins. Quat. Geochronol. 51, 72–86. https://doi.org/10.1016/j.quageo.2019.01.001.

Kirshner, A.E., Anderson, J.B., Jakobsson, M., O'Regan, M., Majewski, W., Nitsche, F.O., 2012. Post-LGM deglaciation in Pine Island Bay, West Antarctica. Quat. Sci. Rev. 38, 11–26.

Lambeck, K., Rouby, H., Purcell, A., Sun, Y., Sambridge, M., 2014. Sea level and global ice volumes from the Last Glacial Maximum to the Holocene. Proc. Natl. Acad. Sci. USA 111, 15296–15303.

Larter, R.D., Anderson, J.B., Graham, A.G.C., Gohl, K., Hillenbrand, C.-D., Jakobsson, M., Johnson, J.S., Kuhn, G., Nitsche, F.O., Smith, J.A., Witus, A.E., Bentley, M.J., Dowdeswell, J.A., Ehrmann, W., Klages, J.P., Lindow, J., Ó Cofaigh, C., Spiegel, C., 2014. Reconstruction of changes in the Amundsen Sea and Bellingshausen Sea sector of the West Antarctic Ice Sheet since the Last Glacial Maximum. Quat. Sci. Rev. 100, 55–86.

LeMasurier, W.E., Harwood, D.M., Rex, D.C., 1994. Geology of Mount Murphy Volcano: an 8-m.y. history of interaction between a rift volcano and the West Antarctic ice sheet. Geol. Soc. Am. Bull. 106, 265–280.

Lindow, J., Castex, M., Wittmann, H., Johnson, J.S., Lisker, F., Gohl, K., Spiegel, C., 2014. Glacial retreat in the Amundsen Sea sector, West Antarctica – first cosmogenic evidence from central Pine Island Bay and the Kohler Range. Quat. Sci. Rev. 98, 166–173.

Liu, Z., Otto-Bliesner He, F., Brady, E.C., Tomas, R., Clark, P.U., Carlson, A.E., Lynch-Stieglitz, J., Curry, W., Brook, E., Erickson, D., Jacob, R., Kutzbach, J., Cheng, J., 2009. Transient simulation of last deglaciation with a new mechanism for Bølling-Allerød warming. Science 325, 310–314.

Mouginot, J., Rignot, E., Scheuchl, B., 2014. Sustained increase in ice discharge from the Amundsen Sea Embayment, West Antarctica, from 1973 to 2013. Geophys. Res. Lett. 41, 1576–1584.

Peltier, W.R., Argus, D.F., Drummond, R., 2015. Space geodesy constrains ice age terminal deglaciation: the global ICE-6G_C (VM5a) model. J. Geophys. Res., Solid Earth 120, 450–487.

Pigati, J.S., Lifton, N.A., Jull, A.J.T., Quade, J., 2010. Extraction of in situ cosmogenic ^{14}C from olivine. Radiocarbon 52 (2–3), 1244–1260.

Pollard, D., Chang, W., Haran, M., Applegate, P., DeConto, R., 2016. Large-ensemble modelling of last deglacial retreat of the West Antarctic Ice Sheet: comparison of simple and advanced statistical techniques. Geosci. Model Dev. 9, 1697–1723.

Pritchard, H.D., Arthern, R.J., Vaughan, D.G., Edwards, L.A., 2009. Extensive dynamic thinning on the margins of the Greenland and Antarctic ice sheets. Nature 461, 971–975.

Rignot, E., Mouginot, J., Scheuchl, B., 2011a. Ice flow of the Antarctic Ice Sheet. Science 333, 1427–1430.

Rignot, E., Mouginot, J., Scheuchl, B., 2011b. MEaSUREs InSAR-Based Antarctica Ice Velocity Map, Version 1. Boulder, Colorado, USA. NASA National Snow and Ice Data Center Distributed Active Archive Center. doi: https://doi.org/10.5067/MEASURES/CRYOSPHERE/nsidc-0484.001, 27 May 2019.

Rignot, E., Mouginot, J., Scheuchl, B., 2011c. Antarctic grounding line mapping from differential satellite radar interferometry. Geophys. Res. Lett. 38, L10504.

Rignot, E., Mouginot, J., Morlighem, N., Seroussi, H., Scheuchl, B., 2014. Widespread, rapid grounding line retreat of Pine Island, Thwaites, Smith, and Kohler glaciers, West Antarctica, from 1992 to 2011. Geophys. Res. Lett. 41, 3502–3509. https://doi.org/10.1002/2014GL060140.

Rignot, E., Mouginot, J., Scheuchl, B., van den Broeke, M., van Wessem, M.J., Morlighem, M., 2019. Four decades of Antarctic Ice Sheet mass balance from 1979–2017. Proc. Natl. Acad. Sci. USA. https://doi.org/10.1073/pnas.1812883116.

Rocchi, S., Le Masurier, W.E., Di Vincenzo, G., 2006. Oligocene to Holocene erosion and glacial history in Marie Byrd Land, West Antarctica, inferred from exhumation of the Dorrel Rock intrusive complex and from volcano morphologies. Geol. Soc. Am. Bull. 118, 991–1005.

Saunders, K.M., Roberts, S.J., Perren, B., Butz, C., Sime, L., Davies, S., Van Nieuwenhuyze, W., Grosjean, M., Hodgson, D.A., 2018. Holocene dynamics of the Southern Hemisphere westerly winds and possible links to CO2 outgassing. Nat. Geosci. 11, 650–655.

Scheuchl, B., Mouginot, J., Rignot, E., Morlighem, M., Khazendar, A., 2016. Grounding line retreat of Pope, Smith, and Kohler Glaciers, West Antarctica, measured with Sentinel-1a radar interferometry data. Geophys. Res. Lett. 43. https://doi.org/10.1002/2016GL069287.

Schoof, C., 2007. Ice sheet grounding line dynamics: steady states, stability, and hysteresis. J. Geophys. Res. 112, F03S28. https://doi.org/10.1029/2006JF000664.

Shepherd, A., Gilbert, L., Muir, A.S., Konrad, H., McMillan, M., Slater, T., Briggs, K.H., Sundal, A.V., Hogg, A.E., Engdahl, M., 2019. Trends in Antarctic ice sheet elevation and mass. Geophys. Res. Lett. https://doi.org/10.1029/2019GL082182.

Small, D., Bentley, M.J., Jones, R.S., Pittard, M.L., Whitehouse, P.L., 2019. Antarctic ice sheet palaeo-thinning rates from vertical transects of cosmogenic exposure ages. Quat. Sci. Rev. 206, 65–80.

Smellie, J.L., 2001. Lithofacies architecture and construction of volcanoes erupted in englacial lakes: Icefall Nunatak, Mount Murphy, eastern Marie Byrd Land, Antarctica. Spec. Publ. Int. Assoc. Sedimentol. 30, 9–34.

Smith, J.A., Hillenbrand, C.D., Kuhn, G., Klages, J.P., Graham, A.G.C., Larter, R.D., Ehrmann, W., Morton, S.G., Wiers, S., Frederichs, T., 2014. New constraints on the timing of West Antarctic Ice Sheet retreat in the eastern Amundsen Sea since the Last Glacial Maximum. Glob. Planet. Change 112, 224–237.

Smith, J.A., Andersen, T.J., Shortt, M., Gaffney, A.M., Truffer, M., Stanton, T.P., Bindschadler, R., Dutrieux, P., Jenkins, A., Hillenbrand, C.-D., Ehrmann, W., Corr, H.F.J., Farley, N., Crowhurst, S., Vaughan, D.G., 2017. Sub-ice-shelf sediments record history of twentieth-century retreat of Pine Island Glacier. Nature 541, 77–80. https://doi.org/10.1038/nature20136.

Stone, J.O., Balco, G., Sugden, D., Caffee, M., Sass III, L., Cowdery, S., Siddoway, C., 2003. Holocene deglaciation of Marie Byrd Land, West Antarctica. Science 299, 99–102.

Whitehouse, P.L., Bentley, M.J., Milne, G.A., King, M.A., Thomas, I.D., 2012. A new glacial isostatic adjustment model for Antarctica: calibrated and tested using observations of relative sea-level change and present-day uplift rates. Geophys. J. Int. 190, 1464–1482.

Wilch, T.I., 1997. Volcanic record of the West Antarctic Ice Sheet in Marie Byrd Land. PhD thesis, Department of Earth & Environmental Science, New Mexico Institute of Mining and Technology, Socorro, USA. Available at: http://www.ees.nmt.edu/outside/alumni/papers/1997d_wilch_ti.pdf. (Accessed 20 November 2018).

Wilch, T.I., McIntosh, W.C., 2002. Lithofacies analysis and 40Ar/39Ar geochronology of ice-volcano interactions at Mt. Murphy and the Crary Mountains, Marie Byrd Land, Antarctica. In: Smellie, J.L., Chapman, M.G. (Eds.), Volcano-Ice Interaction on Earth and Mars. In: Geological Society of London, Special Publication, vol. 202, pp. 237–253.

Yu, H., Rignot, E., Seroussi, H., Morlighem, M., 2018. Retreat of Thwaites Glacier, West Antarctica, over the next 100 years using various ice flow models, ice shelf melt scenarios and basal friction laws. Cryosphere 12, 3861–3876.